

# High-pressure X-ray diffraction study on $\alpha$ -PbF<sub>2</sub>

L. Ehm <sup>a,\*</sup>, K. Knorr <sup>a</sup>, F. Madler <sup>b</sup>, H. Voigtlander <sup>a</sup>,  
E. Busetto <sup>c</sup>, A. Cassetta <sup>c</sup>, A. Lausi <sup>c</sup> & B. Winkler <sup>d</sup>

<sup>a</sup>*Institut fur Geowissenschaften, Mineralogie,  
Christian-Albrechts-Universitat zu Kiel,  
Olshausenstrae 40, D-24098 Kiel, Germany*

<sup>b</sup>*Hahn-Meitner-Institut, Department I/DN,  
Glienicke Strae 100, D-14109 Berlin, Germany*

<sup>c</sup>*ELETTRA, Sincrotrone Trieste,  
Strada Statale 14 - km 163,5 in AREA Science Park,  
I-34012 Basovizza, Italy*

<sup>d</sup>*Institut fur Mineralogie, Kristallographie,  
Johann Wolfgang Goethe-Universitat,  
Senckenberganlage 30, D-60054 Frankfurt am Main, Germany*

---

## Abstract

The high-pressure behaviour of  $\alpha$ -PbF<sub>2</sub> has been investigated by angular-dispersive synchrotron X-ray powder diffraction up to 6.55(8) GPa. The fit of a 3<sup>rd</sup>-order Birch-Murnaghan equation-of-state gave the volume at zero pressure  $V_0=194.14(4)$  Å<sup>3</sup> and the bulk modulus  $b_0=47.0(6)$  GPa with the pressure derivative  $b'=7.9(4)$ . The continuous-symmetry-measure approach has been used for the quantification of the distortion of the coordination polyhedron in  $\alpha$ -PbF<sub>2</sub> revealing an increasing distortion with pressure.

*Key words:* C. high pressure, C. X-ray diffraction, A. inorganic compounds  
*PACS:* 61.10.N2, 62.50.+P, 64.20.+t, 07.35, 61.10.-i

---



---

\* Corresponding author  
*Email address:* ehm@min.uni-kiel.de (L. Ehm ).

## 1 Introduction

Lead fluoride can be found in two polymorphs at ambient conditions:  $\beta$ -PbF<sub>2</sub> in the fluorite type structure [1] and  $\alpha$ -PbF<sub>2</sub> in the orthorhombic cotunnite type structure (fig. 1) with space group  $Pnma$  and  $a=6.440$  Å,  $b=3.899$  Å, and  $c=7.651$  Å [2]. The structure is built up by corrugated layers of tricapped trigonal PbF<sub>9</sub> prisms along  $a$  sharing an edge parallel to the  $b$  direction. All atoms occupy the Wyckoff position  $4c$  ( $x, 1/4, z$ ) with  $x=0.2527(13)$ ,  $z=0.1042(7)$  for Pb,  $x=0.8623(21)$ ,  $z=0.0631(15)$  for F(1) and  $x=0.4662(20)$ ,  $z=0.8457(17)$  for F(2), respectively [2].

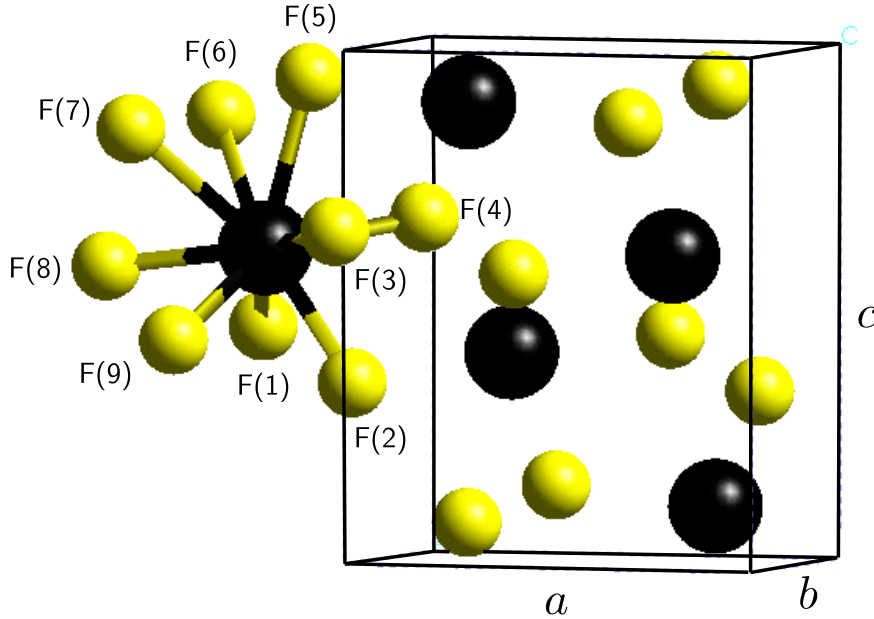


Fig. 1. Schematic drawing of the  $\alpha$ -PbF<sub>2</sub> crystal structure. The black spheres represent Pb<sup>2+</sup> and the gray ones F<sup>-</sup>. The first coordination shell around Pb<sup>2+</sup> is shown where at F(1), (5), (8), (9) and F(2), (3), (4), (6) and (7) occupy symmetrically equivalent positions.

It is not clear which polymorph is thermodynamically stable at ambient conditions. In recent years both phases have intensively been studied due to their potential industrial applications [3,4,5,6,7,8,9,10].  $\beta$ -PbF<sub>2</sub> shows a high superionic conductivity with a low superionic transition temperature suitable for solid state batteries and sensors [5]. The  $\alpha$ -phase is a strong scintillator useful in detector technology [7]. The high-pressure behaviour of PbF<sub>2</sub> has been studied recently by various experimental and theoretical techniques. Lorenzana *et al* [8] investigated the high-pressure properties of PbF<sub>2</sub> by Raman spectroscopy

in conjunction with a first principles, full-potential linear muffin-tin orbital total energy method in the pressure range from ambient pressure up to 30 GPa. The authors detected a phase transition at approximately 0.5 GPa from the cubic  $\beta$ -PbF<sub>2</sub> to the orthorhombic  $\alpha$ -PbF<sub>2</sub>. At 14.7(5) GPa a second phase transition to  $\gamma$ -PbF<sub>2</sub> with a yet unknown structure has been observed. Considering previously investigated high-pressure phases of isotype ionic AX<sub>2</sub> compounds (e.g. SnCl<sub>2</sub>, PbCl<sub>2</sub>, BaCl<sub>2</sub> and BaF<sub>2</sub> [11,12,13]), Lorenzana *et al* proposed a hexagonal Ni<sub>2</sub>In type structure and a monoclinic structure with a doubled *a* axis as possible structures for  $\gamma$ -PbF<sub>2</sub>. Their calculations revealed that above 16.4 GPa, PbF<sub>2</sub> in the Ni<sub>2</sub>In type structure is more stable than  $\alpha$ -PbF<sub>2</sub>. However,  $\gamma$ -PbF<sub>2</sub> in a hexagonal symmetry could not explain the observed Raman spectra and consequently, the authors proposed the monoclinic structure for the high-pressure  $\gamma$  polymorph. High-pressure and high-temperature neutron diffraction experiments have been performed from ambient conditions up to pressures of 1 GPa and temperatures of 966 K to investigate the phase diagram and to determine the nature of the disorder of the fluorine ions at high temperature and its pressure dependence within the  $\alpha$  and  $\beta$  polymorphs of PbF<sub>2</sub> [9]. The phase stability of PbF<sub>2</sub> under high-pressure has also been studied by *ab initio* calculations using the perturbed ion method [10]. The calculations have been performed for the  $\alpha$  and  $\beta$  polymorphs as well as for the two proposed  $\gamma$ -PbF<sub>2</sub> structures. The results of the calculations support the existence of  $\gamma$ -PbF<sub>2</sub> in the hexagonal Ni<sub>2</sub>In type structure above 20.2 GPa. Experimentally determined high-pressure data are mainly for cubic  $\beta$ -PbF<sub>2</sub> [8,9]. Hence, the goal of the work presented here was to measure the structural changes induced by high-pressures in order to elucidate the compression mechanism of  $\alpha$ -PbF<sub>2</sub> and to extend the limited pressure range of the study of Hull and Keen [9] for a precise determination of the equation-of-state. Here we present the results of a high-pressure synchrotron powder diffraction study of  $\alpha$ -PbF<sub>2</sub> up to 6.55 GPa.

## 2 Experimental

The X-ray diffraction experiments were performed using a commercial (Merck, omnipur) polycrystalline sample of PbF<sub>2</sub>. By conventional X-ray powder diffraction it was found that the sample is pure  $\alpha$ -PbF<sub>2</sub>. High-pressure powder diffraction experiments up to 6.55(8) GPa were performed at the wiggler beam-line 5.2R at the ELETTRA synchrotron in Trieste, Italy. The beam-line optic consists of a Si(111) double-crystal monochromator in non-dispersive configuration followed by a three-segment platinum-coated toroidal focusing mirror with a horizontal acceptance of 2.8 mrad. The incident beam was collimated to 80  $\mu$ m diameter. High-pressure powder diffraction patterns were collected at the wavelength  $\lambda=0.6888$  Å using a marresearch (mar345) image plate de-

tector with a pixel-size of  $100 \times 100 \mu\text{m}$ . The exposure time per image was about 20 minutes. Pressure was applied using a Diacell DXR-6 diamond anvil cell mounted on a  $xz$ -positioning-stage for the adjustment in the incident beam. The sample was placed in the hole ( $\varnothing = 150 \mu\text{m}$ ) of an Inconel gasket preindented to  $100 \mu\text{m}$ . In order to ensure hydrostatic conditions a 16:3:1 methanol-ethanol-water mixture was used as pressure transmitting fluid [15]. We used the ruby fluorescence method for the pressure determination applying the Piermarini pressure scale [16]. The sample to detector distance was determined by measuring the sample in the uncompressed cell. Geometry parameters for the radial integration of the two-dimensional data were determined using FIT2D [17]. For the transformation into standard one-dimensional powder patterns the software TWO2ONE [18] was used, which allows for counting statistics of multiply measured data points in order to provide proper error estimates of the intensities and hence, a correct weighting scheme in subsequent least-squares refinements [19]. The one-dimensional powder patterns were corrected for attenuation by the pressure cell. Lattice parameters were obtained from profile matching and the structure was refined at five different pressures by the Rietveld method employing the program FULLPROF [20]. The background was described by a linear interpolation between selected points and the peak profile was modelled using a pseudo-Voigt function [21]. The structural parameters from Boldrini and Loopstra [2] were taken as the initial values for the refinements. The isotropic displacement parameters ( $U_{iso}$ ) for lead and the two fluorine atoms were determined from the measurement at ambient pressure and assumed to be constant in the observed pressure range. The standard deviations of the refined parameters were scaled with the Berar-factor [22]. The pressure-volume data were fitted by a 3<sup>rd</sup>-order Birch-Murnaghan equation-of-state [25]. Since pressure and volume are subject to experimental errors, which have to be weighted correctly in the fit procedure, the conventional least-squares fit is not appropriate. Consequently, the method of orthogonal distance regression (ODR) was used and the equation-of-state implemented in the program code ODRPACK [23,24] to minimise

$$\sum_i (w_{p,i}(p_i^o - p_i^c))^2 + (w_{V,i}(V_i^o - V_i^c))^2, \quad (1)$$

with weights  $w_{p,i} = c_1/\sigma_{p_i^o}^2$  and  $w_{V,i} = c_2/\sigma_{V_i^o}^2$ . The parameters  $c_{1,2}$  are adjustable parameters ensuring that the weighted experimental errors  $w$  are in the same order of magnitude for both variables [24]. The difference between the observed and the calculated values for  $p_i$  and  $V_i$  are at least one order of magnitude smaller than the experimental error bars, when the experimental error bars are used as weights in the fit-procedure. This indicates that the relative precision of the observed data points, which influences the fit, is higher than that represented by the error bars. Taking the differences  $\Delta p$  and  $\Delta V$  between the observations and the equation-of-state as weighted errors in the subsequent fitting cycle did not affect the values of the fitted parameters

themselves but their error estimates.

### 3 Results and Discussion

As an example the observed and calculated diffraction patterns resulting from the Rietveld refinement of the 3.8(1) GPa data are presented in Figure 2. The pressure dependence of the normalised lattice parameters  $a/a_0$ ,  $b/b_0$ ,  $c/c_0$  and the unit cell volume are shown in Figures 3 and 4, respectively. In Table 1 the lattice parameters and the residuals resulting from the Rietveld refinement at five selected pressures are given. The refined atomic positions and the resulting bond distances are given in Tables 2 and 3, respectively. The atomic displacement parameters ( $U_{iso}$ ) were refined to 0.027(3) Å<sup>2</sup> and 0.029(2) Å<sup>2</sup> for lead and the two fluorine ions, respectively

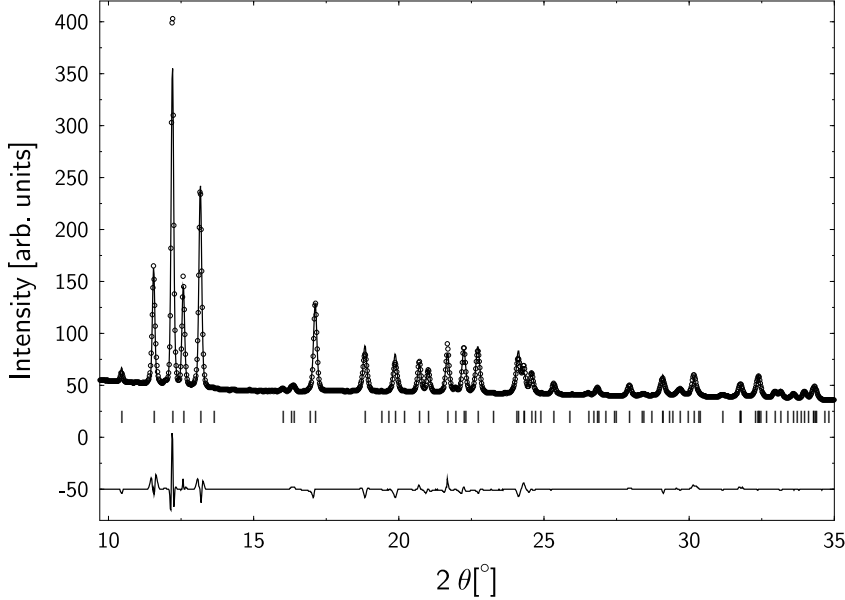


Fig. 2. Observed (circles) and calculated (solid line) diffraction pattern for  $\alpha$ -PbF<sub>2</sub> at 3.8(1) GPa. The difference and the tick marks for the calculated reflection positions are plotted at the bottom of the figure.

The compression of  $\alpha$ -PbF<sub>2</sub> is extremely anisotropic. The compression parallel to the  $a$  axis is 1.5 times larger than that parallel to the  $b$  axis and twice as large as along the  $c$  direction. The volume at zero pressure  $V_0=194.14(4)$  Å<sup>3</sup>, the bulk modulus  $b_0=47.0(6)$  GPa and its pressure derivative  $b'=\partial b/\partial p=7.9(4)$  were determined from the equation-of-state fit.

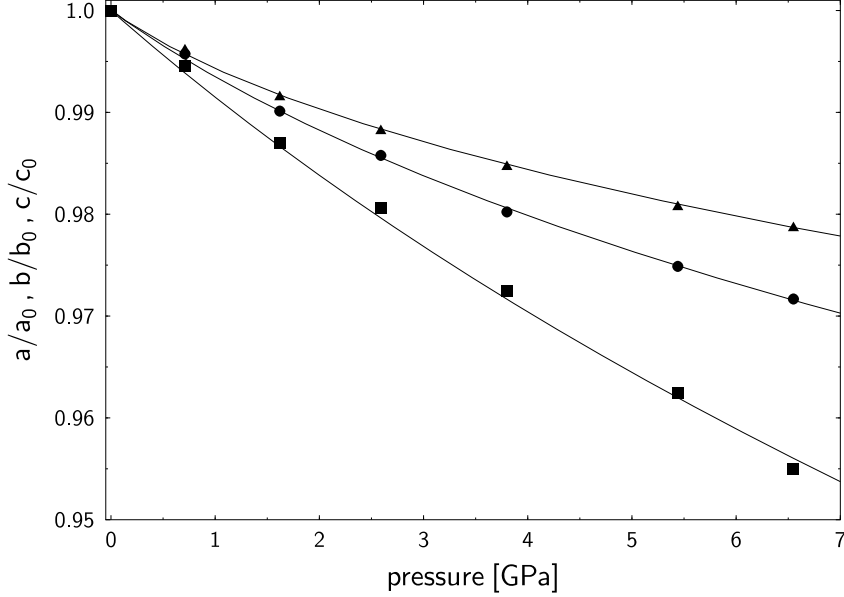


Fig. 3. Evolution of the normalised lattice parameter with pressure. The compression in the three lattice directions  $a$  (■),  $b$  (●) and  $c$  (▲) is anisotropic. The experimental error bars for the pressure and the lattice parameters correspond to the size of the symbols. The lines are curve fittings of 3<sup>rd</sup>-order Birch-Murnaghan equation-of-states to the data.

These results compare to  $V_0 = 198.48 \text{ \AA}^3$ ,  $b_0 = 40 \text{ GPa}$  and  $b' = 4.8$  derived from quantum mechanical calculations at the density functional theory level [8] and with  $b_0 = 57.87 \text{ GPa}$  and  $b' = 4.98$  derived from Hartree-Fock calculations [10] within the accuracy usually obtained in such types of calculations [26,27]. The bulk modulus for  $\alpha\text{-PbF}_2$  of 117(4) GPa reported by Hull and Keen [9] differs significantly from the value derived in this work. However, this difference can be attributed to the limited pressure range and the linear fitting of the volume data for the determination of the bulk modulus in the work by Hull and Keen [9]. The values for the  $b_0$  and  $b'$  obtained in this work are in the same order of magnitude as found for other halides crystallising in the cotunnite type structure, e.g.  $\text{PbCl}_2$  with  $b_0 = 34(1) \text{ GPa}$  and  $b' = 7.4(6)$  [13] and  $\text{CaCl}_2$  with a  $b_0 = 51 \text{ GPa}$  [14].

The changes of the atomic positional parameters in the investigated pressure range are small. The Pb-F distances in the tricapped trigonal prism range from 2.38(2) to 3.12(3) Å at ambient conditions (Tab. 3). The mean of the Pb-F distance in the coordination polyhedron (2.66(2) Å) is close to the sum of the ionic radii [28] for  $\text{Pb}^{2+}$  (1.35 Å) in ninefold- and  $\text{F}^-$  (1.33 Å) in fourfold-coordination. Under a pressure of 6.55(8) GPa the average Pb-F distance is

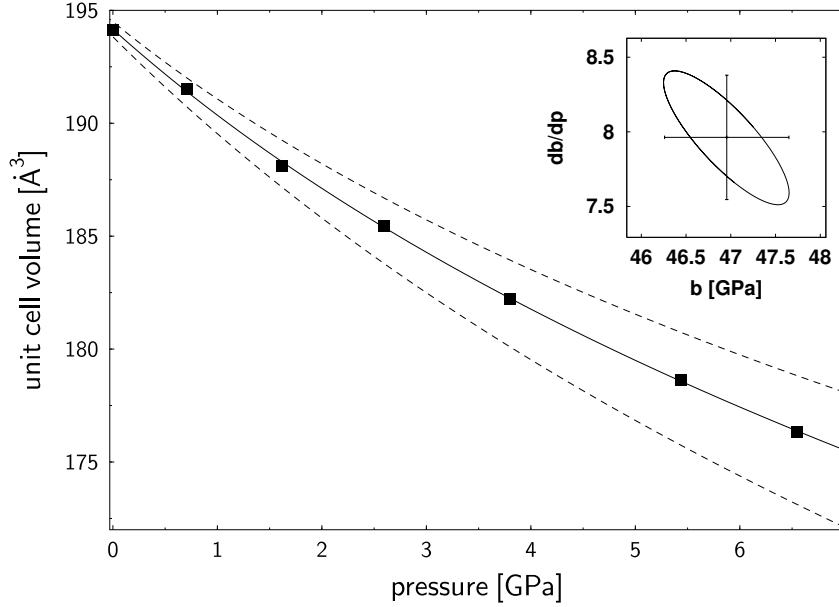


Fig. 4. Pressure dependence of the unit cell volume of  $\alpha$ -PbF<sub>2</sub>. The solid line results from the fit of a 3<sup>rd</sup>-order Birch-Murnaghan equation-of-state, dashed lines represent the 95 % confidence region of the fitted equation-of-state. The experimental error bars correspond to the size of the symbols. The insert shows the one-sigma error ellipsoid of  $b_0$  and  $b'$  for the fit.

reduced to 2.59(2) Å. The individual Pb-F bonds show a different compression behaviour. The following notation of the fluorine ions is according to fig. 1. The bonds in the  $ab$ -plane decrease by 3.64 %, 7.34 % and 0.8 % for Pb-F(1), Pb-F(3) and Pb-F(8), respectively. The Pb-F(2) bond is increased by 4.62 %, Pb-F bonds oriented along the  $c$  direction are less compressible. The Pb-F(5) and the Pb-F(6) bonds are shortened by 1.8 % and 2.88 % at 6.55(8) GPa.

The structural changes in a compound under high-pressure can be described by considering the distortion of the respective coordination polyhedron. Recently, two different approaches have been developed [29,30] to quantify the distortion of a polyhedron by comparison of an ideal to the real one.

The capped square anti-prism and the tricapped trigonal prism (TTP) are ideal polyhedra for a nine-fold coordination [31]. The TTP is found in  $\alpha$ -PbF<sub>2</sub>. The regular TTP, shown in fig. 5, is characterised as follows: all nine ligands are located on the surface of a sphere with radius  $r_s$ , and the polyhedra edge lengths are  $AB=AC=2r_s/\sqrt{3}$  and  $AD=2r_s/3\sqrt{5}$  [31]. The distortion measure of Mackovicky and Balić-Žunić [29] indicates the volume difference between real and ideal coordination polyhedra. Therefore the ligands of the real and ideal polyhedra have to be located on a common circumsphere with

Table 1

Residuals, lattice and profile parameters from Rietveld refinement for selected pressures.

p [GPa]	0.00(4)	1.62(5)	3.80(9)	5.44(9)	6.55(8)
$R_{wp}$ %	11.1	15.0	14.1	11.3	13.6
$\chi^2$	1.93	3.44	3.87	2.53	2.16
$a$ [Å]	6.4567(9)	6.372(2)	6.278(1)	6.213(1)	6.165(1)
$b$ [Å]	3.9071(5)	3.8680(9)	3.8294(8)	3.8088(8)	3.7963(8)
$c$ [Å]	7.666(1)	7.603(2)	7.549(2)	7.520(1)	7.503(2)
$\eta$	0.13(4)	0.07(3)	0.25(4)	0.14(3)	0.09(4)
U	-0.19(9)	-0.17(5)	-0.85(2)	-0.53(1)	-0.47(3)
V	0.14(2)	0.16(7)	0.39(3)	0.29(3)	0.27(4)
W	0.0034(3)	0.006(2)	0.017(2)	0.010(2)	0.009(5)

Table 2

Atomic positions resulting from Rietveld refinements.

	Pb		F(1)		F(2)	
	$x$	$z$	$x$	$z$	$x$	$z$
0.00(4) [GPa]	0.254(3)	0.1067(5)	0.891(7)	0.051(7)	0.489(8)	0.850(6)
1.62(5) [GPa]	0.253(4)	0.1111(7)	0.880(9)	0.03(2)	0.49(1)	0.850(9)
3.80(9) [GPa]	0.251(5)	0.1139(8)	0.89(1)	0.02(1)	0.50(1)	0.854(9)
5.44(9) [GPa]	0.253(4)	0.1145(6)	0.888(9)	0.041(7)	0.477(9)	0.853(8)
6.55(8) [GPa]	0.254(4)	0.1163(7)	0.884(9)	0.037(9)	0.51(1)	0.843(9)

radius  $r_s$ . However, this measure is not applicable to polyhedra with a large variation in the bond distances as found in  $\alpha$ -PbF<sub>2</sub>. Hence, the distortion measure based on the continuous symmetry measure (CSM) [30] was used. In this method a regular tricapped trigonal prism is embedded in the observed one. As an additional free parameter the radius around the three cap atoms  $r_e$  was used to consider non-spherical deformation. In order to find the best conformation, an evolution strategy [32] was used to minimise the euclidean norm (instead of the standard least-squares method employed by Pinsky and Avnir [30], which requires the computation of the two-dimensional derivative with respect to  $r_s$  and  $r_e$ ). For various pressures the results of the embedding are given in table 4. At ambient pressure the TTP is slightly distorted (CSM=1.378) compared to the ideal value (CSM=1). The nine fluorine ions are not arranged on the surface of a sphere ( $r_q=1$ ) but on an ellipsoid of revolution ( $r_q=1.062$ ). Remarkably, the lead ion is not located in the conjoined



Table 3

Bond distances in the coordination shell around a lead atom (see fig. 1. The values are given in Å.

p [GPa]	0.00(4)	1.62(5)	3.80(9)	5.44(9)	6.55(8)
Pb-F(1,9)	2.47(2)	2.40(1)	2.35(2)	2.39(2)	2.38(2)
Pb-F(2)	2.48(2)	2.53(2)	2.51(3)	2.41(3)	2.60(3)
Pb-F(3,4)	2.59(3)	2.51(3)	2.49(3)	2.55(2)	2.40(2)
Pb-F(5)	2.77(2)	2.78(3)	2.88(2)	2.72(1)	2.72(3)
Pb-F(6,7)	3.12(3)	3.10(2)	3.06(3)	2.98(2)	3.03(3)
Pb-F(8)	2.38(2)	2.44(2)	2.36(2)	2.36(1)	2.36(2)

Table 4

Evolution of the tricapped trigonal prism coordination polyhedra in  $\alpha$ -PbF<sub>2</sub> with pressure. Tabulated are: The mean fluorine distance  $d_{mF}$  from the centroid, the scattering of the fluorine distances around the mean  $\sigma$ , the distance  $Pb_{exc}$  between the lead ion and the centroid of the nine fluorine ions, the minimal distance  $d$  and the mean distance per coordinate  $d/coord$  between observed and embedded ideal polyhedra. The distortion is given in the continuous symmetry measure CSM [30] and the quotient  $r_q=r_s/r_e$  of the radii around the circumscribed sphere ( $r_s$ ) and caps ( $r_e$ ).

p [GPa]	$d_{mF}$ [Å]	$\sigma$ [Å]	$Pb_{exc}$ [Å]	$d$ [Å]	$d/coord$ [Å]	CSM	$r_q$
0.00(4)	2.6574	0.557	0.3049	0.8803	0.033	1.378	1.062
1.62(5)	2.6324	0.564	0.3002	0.9350	0.035	1.492	1.024
3.80(9)	2.6098	0.598	0.3023	1.1464	0.042	1.859	1.003
5.44(9)	2.5857	0.477	0.2458	0.8787	0.033	1.455	1.052
6.55(8)	2.5767	0.627	0.2849	0.9667	0.036	1.607	1.006

centroid of the fluorine ligands. The variance of the fluorine bond distances increase with pressure, reflecting the difference in the compression of the individual Pb-F bonds. The lead ion shifts towards the TTP-centroid, and the arrangement of the fluorine ligands becomes more spheric with pressure. However, the minimal distance between the observed and the embedded fluorine ions increases. Compared to TTP the distortion is larger and the spheroidal arrangement of the fluorine ligands extends, both effects can be attributed to increasing angular distortions.

Raman spectroscopy measurement above 14.7 GPa in PbF<sub>2</sub> indicate a structural phase transition to a post-cotunnite structure with monoclinic symmetry [8] as observed in the isotype SnCl<sub>2</sub> and PbCl<sub>2</sub> compounds [13]. The extrapolation of the CSM to higher pressures indicate a increasing distortion of the

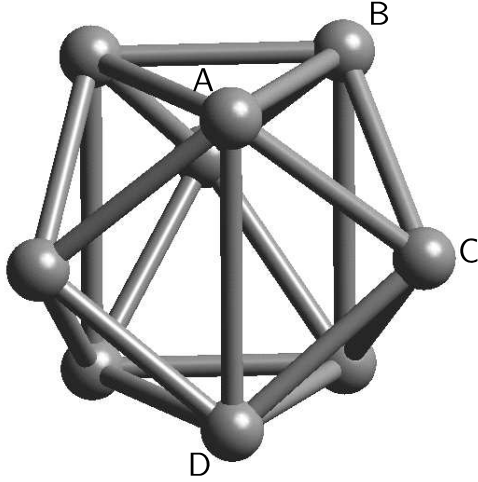


Fig. 5. The regular tricapped trigonal prism with all ligands located on a sphere with radius  $r_s$ . The polyhedral edge lengths are  $AB=AC=2r_s/\sqrt{3}$  and  $AD=2r_s/3\sqrt{5}$ .

TTP polyhedron. However, from the present CSM data a saturation of the CSM may not be excluded. Such a behaviour would suggest a ridged-unit like behaviour of the TTP as it can be found e.g. for the tetrahedral building units in silicates. Since the structure of the post-cotunnite phase is not known for  $\text{PbF}_2$ , a further examination of the high-pressure behaviour seems to be justified.

## 4 Acknowledgements

LE, KK and HV would like to thank the European Union for financial support under the TMR program. We are grateful to Korth Kristalle GmbH Kiel for the donation of the sample and to the German Science Foundation (DFG) for funding under grant Wi-1232/10.

## References

- [1] P. Byström, The structure of fluorides and oxifluoride of bivalent lead, *Arkiv för Chemi, Mineralogi och Geologi A* 24 (1947), 1.
- [2] P. Boldrini and B.O. Loopstra, Neutron diffraction investigations of orthorhombic lead(II)fluoride, *Acta Cryst.* 22 (1967), 744.
- [3] G.A. Samara, Temperature and pressure dependence of the dielectric properties of  $\text{PbF}_2$  and the alkaline-earth fluorides, *Phys. Rev. B* 13 (1976), 4529.

- [4] J. Oberschmidt, Effect of Frenkel defects on the high-pressure phase transitions in  $\text{PbF}_2$  and  $\text{SrCl}_2$ , *Phys. Rev. B* 24 (1981), 3584.
- [5] S. Chandra, *Superionic solids: Principles and applications*, North-Holland Publ. Co, Amsterdam, 1981.
- [6] T.S. Aurora, D.O. Peterson and S.M. Day, Thermal-expansion and index-of-refraction variation in lead fluoride between 300 and 850 K, *Phys. Rev. B* 41 (1990), 9647.
- [7] D.L. Alov and S.I. Rybchenko, Luminescence of orthorhombic  $\text{PbF}_2$ , *J. Phys. Condens. Matter* 7 (1995), 1475.
- [8] H.E. Lorenzana, J.E. Klepeis, M.J. Lipp, W.J. Evans, H.B. Radousky and M. van Schilfgaard, High-pressure phases of  $\text{PbF}_2$ : A joint experimental and theoretical study, *Phys. Rev. B* 56 (1997), 543.
- [9] S. Hull and D.A. Keen, Effect of hydrostatic pressure on the crystal structure and superionic behavior of lead(II)fluoride, *Phys. Rev. B* 58 (1998), 14837.
- [10] A. Costales, M.A. Blanco, R. Pandey and J.M. Recio, Theoretical characterization of the high-pressure phases of  $\text{PbF}_2$ , *Phys. Rev. B* 61 (2000), 11359.
- [11] J.M. Leger, J. Haines and A. Atouf, High-pressure transitions to a postcotunnite phase in ionic  $\text{AX}_2$  compounds, *Phys. Rev. B* 51 (1995), 3902.
- [12] J.M. Leger, J. Haines, A. Atouf, O. Schulte and S. Hull, High-pressure X-ray- and neutron-diffraction studies of  $\text{BaF}_2$ : An example of a coordination number of 11 in  $\text{AX}_2$  compounds, *Phys. Rev. B* 52 (1995), 13247.
- [13] J.M. Leger, J. Haines and A. Atouf, The high pressure behaviour of the cotunnite and post-cotunnite phases of  $\text{PbCl}_2$  and  $\text{SnCl}_2$ , *J. Phys. Chem. Solids* 57 (1996), 7.
- [14] J.M. Leger, J. Haines and C. Danneels, Phase transition sequence induced by high-pressure in  $\text{CaCl}_2$ , *J. Phys. Chem. Solids* 59 (1998), 1199.
- [15] I. Fujishiro, G.J. Piermarini, S. Block, R.G. Munro, *High Pressure in Research and Industry*, Proceedings of the 8th AIRPT Conference Uppsala, edited by Backman, C.M.; Johannisson, T.; Tegner, L., (1982), 608.
- [16] G.J. Piermarini, S. Block, J.D. Barnett, R.A. Forman, Calibration of the pressure dependence of the  $R_1$  ruby fluorescence line to 195 kbar, *J. Appl. Phys.* 47 (1975), 2774.
- [17] A. Hammersley, S. Svensson, M. Hanfland, A. Fitch and D. Häusermann, Two-dimensional detector software: from real detector to idealised image or two-theta scan, *High Pressure Research* 14 (1996), 235.
- [18] S. Vogel, L. Ehm, K. Knorr, Automated Processing of 2D Powder Diffraction Data, *Adv. X-ray Anal.* in print

- [19] M. Chall, K. Knorr, L. Ehm and W. Depmeier, Estimating intensity errors of powder diffraction from area detectors, *High Pressure Research* 17 (2000), 315.
- [20] J. Rodriguez-Carvajal, Recent advances in magnetic structure determination by neutron powder diffraction, *Physica B* 192 (1993), 55.
- [21] P. Thompson, D. E. Cox and J. B. Hastings, Rietveld refinement of Debye-Scherrer synchrotron X-ray data from  $\text{Al}_2\text{O}_3$ , *J. Appl. Cryst.* 20 (1987), 79.
- [22] J.-F. Berar and P. Lelann, E.s.d.'s and estimated probable error obtained in Rietveld refinements with local correlations, *J. Appl. Cryst.* 24 (1991), 1.
- [23] P.T. Boggs, R.H. Byrd, J. Rogers Donaldson and R.B. Schnabel, ODRPACK Software for weighted orthogonal distance regression, *ACM Transactions on Mathematical Software* 15 (1989), 348.
- [24] P.T. Boggs, R.H. Byrd, J.E. Rogers and R.B. Schnabel, User's reference guide for ODRPACK version 2.01 - Software for weighted orthogonal distance regression, NIST IR 4834, U.S. Government Printing Office (1992).
- [25] F. Birch, Finite strain isotherm and velocities for single-crystal and polycrystalline NaCl at high pressure and 300 K, *J. Geophys. Res.* 83 (1978), 1257.
- [26] B. Winkler, Introduction to computational crystallography, *Z. Kristallogr.* 214 (1999), 506.
- [27] V. Milman, B. Winkler, J.A. Withe, C.J. Pickard, M.C. Payne, E.V. Akhmatkaya and R.H. Nobes, Electronic structure, properties, and phase stabilities of inorganic crystals: a pseudopotential plane-wave study, *Intern. J. Quantum Chem.* 77 (2000), 895.
- [28] R.D. Shannon, Revised effective ionic radii and systematic studies of interatomic distances in halides and chalcogenides, *Acta Cryst. A* 32 (1976), 751.
- [29] E. Makovicky and T. Balić-Žunić, New measurement of distortion for coordination polyhedra, *Acta Cryst. B* 54 (1998), 766.
- [30] M. Pinsky and D. Avnir, Continuous symmetry measures. 5. The classical polyhedra, *Inorg. Chem.* 37 (1998), 5575.
- [31] D.L. Kepert: *Inorganic Stereochemistry*, Springer-Verlag, Berlin/Heidelberg/New York, 1982.
- [32] F. Mädlar, E. Behrends and K. Knorr, A geometric centroid principle and its application, *Acta Cryst. A* 57 (2001), 20.